GEOPHYSICS, VOL. 68, NO. 3 (MAY-JUNE 2003); P. 1065–1074, 14 FIGS.
10.1190/1.1581078

Angle-domain common-image gathers by wavefield continuation methods

Paul C. Sava* and Sergey Fomel‡

ABSTRACT

Migration in the angle domain creates seismic images for different reflection angles. We present a method for computing angle-domain common-image gathers from seismic images obtained by depth migration using wavefield continuation. Our method operates on prestack migrated images and produces the output as a function of the reflection angle, not as a function of offset ray parameter as in other alternative approaches. The method amounts to a radial-trace transform in the Fourier domain and is equivalent to a slant stack in the space domain. We obtain the angle gathers using a stretch technique that enables us to impose smoothness through regularization. Several examples show that our method is accurate, fast, robust, and easy to implement. The main anticipated applications of our method are in the areas of migration-velocity analysis and amplitude-versus-angle analysis.

INTRODUCTION

Traditionally, migration velocity analysis and amplitude-variation-to-offset (AVO) studies employ offset-domain common-image gathers (ODCIG), since most of the relevant information is not described by the zero-offset images. There are two kinds of ODCIGs: those produced by Kirchhoff migration, and those produced by migration by wavefield continuation, commonly referred to as "wave-equation migration," a convention which we occasionally use in this paper. These two kinds of ODCIGs have different meanings. For a perfectly known velocity model, the ODCIGs generated by Kirchhoff migration produce flat events, whereas the ODCIGs generated by wave-equation migration produce events perfectly focused at zero offset. There is no simple relationship between these two types of ODCIGs, one involves the concept of flat gathers, the other involves the concept of focused events. Furthermore, the offset used in the Kirchhoff ODCIGs is a data parameter, whereas the offset used in the wave-equation ODCIGs is a model parameter because it characterizes the migrated image after focusing at the reflection point and not the recorded data.

Wave-equation migration is a powerful and acurate imaging tool in complex areas. However, ODCIGs fail to properly characterize complex propagation paths because, among other things, of the ambiguity of reflector positions caused by multipathing, which make interpretation and migration velocity analysis difficult (Nolan and Symes, 1996).

The problems observed for ODCIGs can be alleviated using angle-domain common-image gathers (ADCIG), which are representations of the seismic images sorted by the incidence angle at the reflection point. ADCIGs can be produced either by using Kirchhoff methods (Xu et al., 1998; Brandsberg-Dahl et al., 1999) or by using wave-equation methods (de Bruin et al., 1990; Prucha et al., 1999; Mosher and Foster, 2000). Unlike ODCIGs, ADCIGs produced with either kind of method have similar characteristics since they simply describe the reflectivity as a function of incidence angle at the reflector (Figure 1). However, Stolk and Symes (2002) argue that even in perfectly known but strongly refracting media, Kirchhoff ADCIGs are hampered by significant artifacts caused by the asymptotic assumptions of ray-based imaging.

This paper focuses on ADCIGs computed in relation with wave-equation migration. Angle gathers can be obtained using wave-equation techniques either for shot-profile migration, as described by de Bruin et al. (1990), or for shot-geophone migration, as described by Prucha et al. (1999) or Mosher and Foster (2000). In both cases, angle gathers are evaluated using slant stacks of the downward-continued wavefield, prior to imaging. We refer to these techniques as "data-space methods" since they involve the downward-continued wavefield before imaging. These data-space methods produce angle gathers as a function of offset ray parameter (p_h), instead of the true reflection angle.

In this paper, we present an alternative method that enables us to compute angle gathers after imaging. We refer to this technique as an "image-space method" because it does not involve the wavefields anymore, but the prestack images

Manuscript received by the Editor October 16, 2001; revised manuscript received September 16, 2002.
*Stanford University, Stanford Exploration Project, Geophysics Department, Mitchell Building, Stanford, California 94305-2215. E-mail: paul.sava@stanford.edu.
‡Formerly Stanford University, Stanford Exploration Project, Geophysics Department, Mitchell Building, Stanford California 94305-2215; presently Bureau of Economic Geology, University of Texas at Austin, Austin, Texas 78713-8924. E-mail: sergey.fomel@beg.utexas.edu.

obtained by imaging at zero time but not at zero offset. We show that this new method directly produces angle gathers as a function of the reflection angle, as opposed to the data-space methods which produce angle gathers as a function of offset ray parameter. The image-space method allows for a convenient, robust, and slightly more efficient implementation than the data-space method. We also show that for both the data-space and image-space methods, the slant-stack transformation can be easily implemented as a radial-trace transform in the frequency-wavenumber domain, as described by Ottolini (1982).

We start by introducing the angle-gather migration concept using traveltime relations for the basic Kirchhoff implementation of prestack time migration. The analysis follows Fowler's general approach to prestack time migration methods (Fowler, 1997). Next, we present our method of computing angle gathers in the image-space from images obtained by wavefield-continuation migration. We then address the issue of regularization of the angle-gather transformation, then present 2D and 3D synthetic and real data examples, and end with a discussion on the differences between the methods used to compute ADCIGs in the data and image spaces.

INTRODUCTION TO ANGLE-GATHER MIGRATION

This section is a brief introduction to the concept of angle-gather migration. Readers familiar with this concept can safely skip to the next section.

Let us consider a simple reflection experiment in a constant velocity medium, as depicted in Figure 2. The pair of incident and reflected rays and the line between the source s and the receiver r form a triangle in space. From the trigonometry of that triangle, we can derive simple relationships among all the variables of the experiment (Fomel, 1997).

Introducing the dip angle α and the reflection angle γ, the total reflection traveltime t can be expressed from the law of sines as

$$t = \frac{2h}{v}\,\frac{\cos(\alpha+\gamma)+\cos(\alpha-\gamma)}{\sin 2\gamma} = \frac{2h}{v}\,\frac{\cos\alpha}{\sin\gamma}, \qquad (1)$$

where v is the medium velocity, and h is half the offset between the source and the receiver.

Additionally, by following simple trigonometry, we can connect the half-offset h with the depth of the reflection point z, as follows:

$$h = \frac{z}{2}\,\frac{\sin 2\gamma}{\cos(\alpha+\gamma)\cos(\alpha-\gamma)} = z\,\frac{\sin\gamma\cos\gamma}{\cos^2\alpha-\sin^2\gamma}. \qquad (2)$$

Finally, the horizontal distance between the midpoint x and the reflection point ξ is

$$x-\xi = h\,\frac{\cos(\alpha-\gamma)\sin(\alpha+\gamma)+\cos(\alpha+\gamma)\sin(\alpha-\gamma)}{\sin 2\gamma} = h\,\frac{\sin\alpha\cos\alpha}{\sin\gamma\cos\gamma} \qquad (3)$$

Equations (1)–(3) completely define the kinematics of angle-gather migration. Regrouping the terms, we can rewrite the three equations in a more symmetric form:

$$t = \frac{2z}{v}\,\frac{\cos\alpha\cos\gamma}{\cos^2\alpha-\sin^2\gamma}, \qquad (4)$$

$$h = z\,\frac{\sin\gamma\cos\gamma}{\cos^2\alpha-\sin^2\gamma}, \qquad (5)$$

$$x-\xi = z\,\frac{\sin\alpha\cos\alpha}{\cos^2\alpha-\sin^2\gamma}. \qquad (6)$$

For completeness, here is the inverse transformation from t, h, and $x-\xi$ to z, γ, and α:

$$z^2 = \frac{[(vt/2)^2-(x-\xi)^2][(vt/2)^2-h^2]}{(vt/2)^2}, \qquad (7)$$

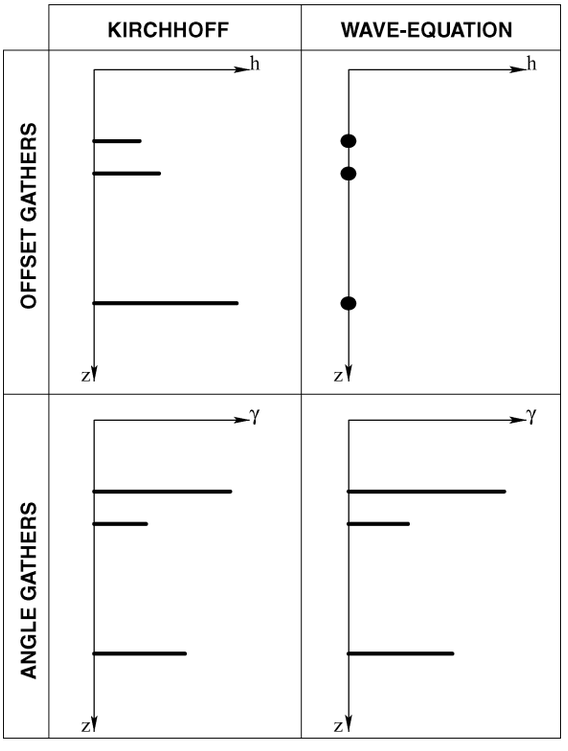

FIG. 1. Offset-domain and angle-domain common image gathers. A schematic comparison between Kirchhoff and wave-equation methods.

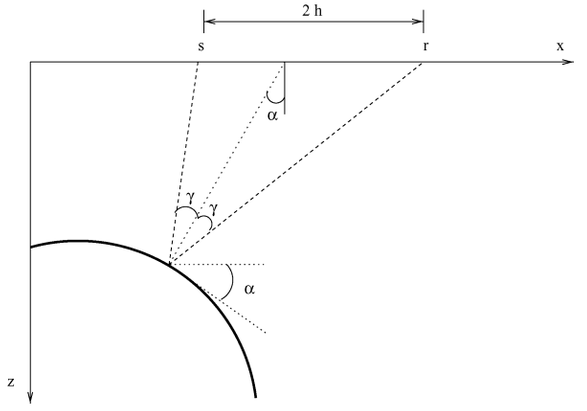

FIG. 2. Reflection rays in a constant-velocity medium.

$$\sin^2\gamma = \frac{h^2[(vt/2)^2 - (x-\xi)^2]}{(vt/2)^4 - h^2(x-\xi)^2}, \tag{8}$$

$$\cos^2\alpha = \frac{(vt/2)^2[(vt/2)^2 - (x-\xi)^2]}{(vt/2)^4 - h^2(x-\xi)^2}. \tag{9}$$

The inverse transformation (7)–(9) can be found by formally solving system (4)–(6).

The lines of constant reflection angle (γ) and variable dip angle (α) for a given position of a reflection (diffraction) point $\{z, \xi\}$ are summation curves for angle-gather Kirchhoff migration. The whole range of such curves for all possible values of γ covers the diffraction traveltime surface "Cheops' pyramid" (Claerbout, 1985) in the $\{t, x, h\}$ space of seismic reflection data. As pointed out by Fowler (1997), this condition is sufficient for proving the kinematic validity of the angle-gather approach. For comparison, Figure 3 shows the diffraction traveltime pyramid from a diffractor at 0.5 km depth. The pyramid is composed of common-offset summation curves of the conventional time migration. Figure 4 shows the same pyramid composed of constant-γ curves of the angle-gather migration.

The most straightforward Kirchhoff algorithm for angle-gather migration in homogeneous media can be formulated as follows:

For each reflection angle γ and each dip angle α,
For each output location $\{z, \xi\}$,

1) Find the traveltime t, half-offset h, and midpoint x from Equations (4), (5), and (6), respectively.
2) Stack the input data values into the output.

As follows from equations (4)–(6), the range of possible α should satisfy the condition

$$\cos^2\alpha > \sin^2\gamma \quad \text{or} \quad |\alpha| + |\gamma| < \frac{\pi}{2}. \tag{10}$$

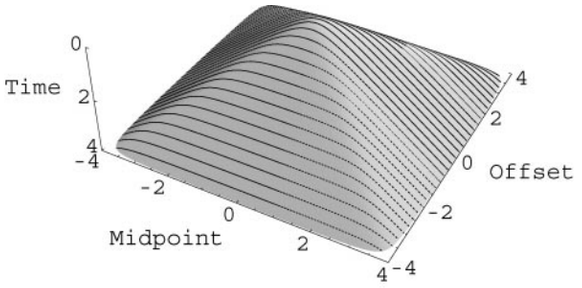

FIG. 3. Traveltime pyramid composed of common-offset summation curves.

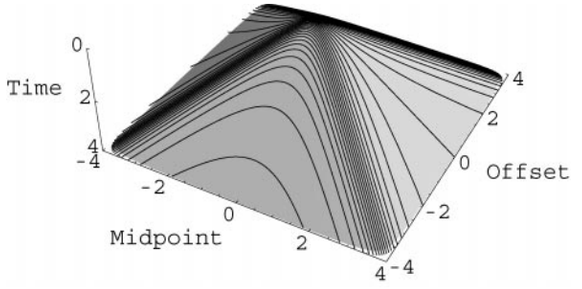

FIG. 4. Traveltime pyramid composed of common-angle summation curves.

The described algorithm is not the most optimal in terms of the input/output organization, but it can serve as a basic implementation of the angle-gather idea. In the next section, we show how to obtain angle-gathers in the frequency domain using wavefield-continuation imaging methods.

ANGLE GATHERS IN THE IMAGE SPACE

Angle gathers can be conveniently formed in the frequency-wavenumber domain using wavefield-continuation imaging methods. If we consider that in constant velocity media, t is the traveltime from the source to the reflector and back to the receiver at the surface, h is half the offset between the source and the receiver, z is the depth of the reflection point, α is the geologic dip, and γ is the reflection angle (Figure 5), we can write

$$\frac{\partial t}{\partial h} = \frac{2\cos\alpha\sin\gamma}{v} \tag{11}$$

and

$$\frac{\partial t}{\partial z} = \frac{2\cos\alpha\cos\gamma}{v}. \tag{12}$$

From Equations (11) and (12), using the implicit functions theorem, we can write

$$\tan\gamma = -\left.\frac{\partial z}{\partial h}\right|_{t,x}, \tag{13}$$

the relation which is the basis for our angle-gather method. The full derivation of Equation (13) is included in Appendix A.

Equation (13) is derived in constant velocity media, but it remains perfectly valid in a differential sense in any arbitrary velocity media if we consider h to be half the offset at the reflector depth. The offset at depth characterizes the downward-continued wavefield and, as Figure 5 shows, this is the offset associated with the wavefield as it approaches the reflection surface and not the surface offset. In this context, the half-offset h can be seen as an image parameter, different from the offset at the surface which is a data parameter.

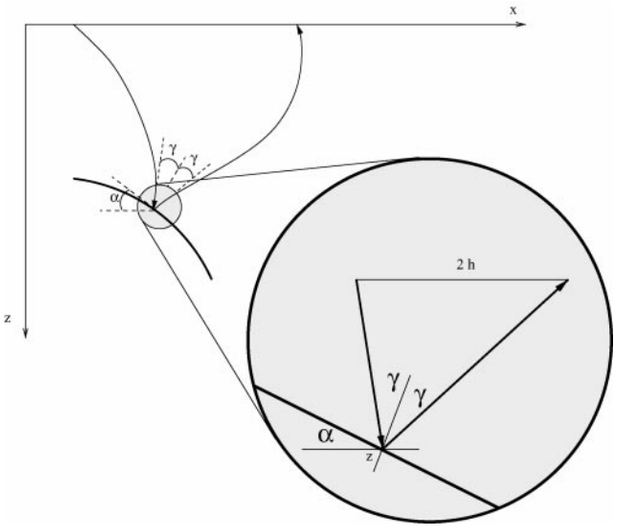

FIG. 5. Reflection rays in an arbitrary-velocity medium.

In the frequency-wavenumber domain, formula (13) takes the simple form

$$\tan\gamma = -\frac{k_h}{k_z}, \tag{14}$$

where k_z and k_h are the depth and frequency wavenumbers, respectively (Weglein and Stolt, 1999).

Equation (14) indicates that angle-gathers can be formed using frequency-domain algorithms. Wave-equation migration is ideally suited to compute angle-gathers using such a method, since the migration output is precisely described by the offset at the reflector depth and not by the surface offset.

We can also recognize that equation (11) simply describes the offset ray parameter (p_h) of the propagating wave at the incidence with the reflector. Using the definition

$$p_h = \left.\frac{\partial t}{\partial h}\right|_{z,x}, \tag{15}$$

it follows that we can write a relation similar to equation (14) to evaluate the offset ray parameter in the Fourier-domain:

$$p_h = \frac{k_h}{\omega}, \tag{16}$$

where ω is the temporal frequency.

Both Equations (14) and (16) can be used to compute image gathers through radial trace transforms in the Fourier domain (Appendix B). The major difference is that Equation (14) operates in the image space, were as Equation (16) operates in the data space.

Other major differences between the two methods are the following:

1) The image-space method is completely decoupled from migration; therefore, conversion to reflection angle can be thought of as a postprocessing after migration. Such postprocessing is useful because it allows conversion from the angle domain back to the offset domain without remigration, a conclusion which does not hold true for the data-space method, where the transformation is a function of the data frequency.
2) The angles we obtain using equation (14) are geometrical measures of the reflection angle. For amplitude-variation-with angle (AVA) purposes, it is convenient to have the reflection amplitudes described as a function of reflection angle and not as a function of offset ray parameter, a case in which conversion to reflection angle requires dip and velocity information, as seen in equation (11). The meaning of the AVA in the ADCIGs created using our method depends on the properties of the migration algorithm from which the common-image gathers are created, but this subject falls outside the scope of this paper Sava et al., 2001). However, one of our examples demonstrate that a correct implementation of our method can preserve the amplitude pattern resulting from migration.
3) Both ADCIGs methods require accurate knowledge of the imaging velocity. The difference is that the data-space method is less sensitive to inaccuracies in the location of sharp velocity boundaries because the conversion to angle-gathers is done at every step as the wavefield is continued in depth. In contrast, the image-space angle gathers are created using the information contained in the entire image gathers; therefore, slight imaging errors at a given depth influence angle gathers at other depth levels. However, conversion from p_h to the reflection angle γ is influenced by errors in the velocity maps as well.

REGULARIZATION OF THE ANGLE DOMAIN

The angle-gather transformation introduced in this paper amounts to a stretch of the offset to reflection angle according to equation (14). The stretch takes every point on the offset wavenumber axis and repositions it on the angle axis, most likely not on its regular grid. We, therefore, need to interpolate the unevenly sampled axis to the regular one. In other words, we need to solve a simple linear interpolation problem:

$$\mathbf{Lm} \approx \mathbf{d}, \tag{17}$$

where the model ($\mathbf{m}$) is represented by the evenly-spaced values on the angle axis, the data ($\mathbf{d}$) is represented by the unevenly-spaced values on the angle axis, and $\mathbf{L}$ represents a 1D linear interpolation operator. Both $\mathbf{m}$ and $\mathbf{d}$ in equation (17) are Fourier-domain quantities. Since parts of the model space will not be covered because of the uneven distribution of the data, we need to regularize the interpolation process and solve a system such as

$$\begin{aligned} \mathbf{Lm} &\approx \mathbf{d} \\ \epsilon\mathbf{Am} &\approx 0, \end{aligned} \tag{18}$$

where ($\mathbf{A}$) represents a 1D roughening operator (1D gradient, for example) and ϵ is a scalar parameter indicating the strength of the regularization term. The least-squares solution to the system (18) takes the usual form

$$\mathbf{m} = (\mathbf{L}^T\mathbf{L} + \epsilon^2\mathbf{A}^T\mathbf{A})^{-1}\mathbf{L}^T\mathbf{d}. \tag{19}$$

In the special case of the angle-domain stretch, the inverted term on the right side of equation (19) is a tridiagonal matrix and can be easily inverted using fast tridiagonal solvers (Golub and Van Loan, 1989). However, given the sparseness of the stretched data, the least-squares tridiagonal matrix corresponding to the operator $\mathbf{L}$ has zeros present along the diagonals, which results in instability during inversion and artifacts in the angle gathers. Regularization fills those gaps, and the inversion of the matrix in Equation (19) is well behaved.

Finally, we emphasize that regularization is not applied in the space domain, but in the Fourier domain, and so our method does not smooth reflection events spatially. Consequently, the amplitude response in ADCIGs is not altered, although, as we noted earlier, there are other reasons why direct AVA interpretation is not straightforward.

EXAMPLES

We exemplify the proposed method on two synthetic models and two real data sets.

The first example represents a simple image gather with one seismic event perfectly focused at zero offset (Figure 6). As expected, conversion to the angle domain produces a flat event, which fattens out at high angles due to the finite sampling of the offset axis. This phenomenon is a consequence of the acquisition geometry and is not a property of the conversion to the angle domain. The top panels of Figure 6 show the amplitude of this simple event as a function of offset (left) and reflection

angle (right). The conversion to angle produces a flat amplitude curve, as expected for this perfectly focused event. If this event is produced using true amplitude migration, then the reflectivity function of angle (AVA) produced by our algorithm is also true amplitude.

The second example is a 2D synthetic model (Figure 7) with dipping reflectors at various angles. We generate the synthetic data using wavefield-continuation modeling and then image it using correct and incorrect velocities. The ADCIGs are flat for the case of correct velocity (Figure 8), but they are not flat for the case of incorrect velocity (Figure 9). The bottom panels show ADCIGs computed in the image and data spaces at the location indicated by the vertical line at 1.2 km. The velocity changes in the upper part of the model from 1.75 km/s in the correct model to 1.5 km/s in the incorrect one. Because we have simulated wide offset data, the deeper flat events do not suffer much from reduced angular coverage. However, the limited acquisition causes a reduction in angular coverage for the steeply dipping fault.

Figures 8 and 9 also show the different amplitude behavior between the image space and data space methods: for the image space method, the amplitudes decrease as a function of angle; for the data space method, the amplitudes increase as a function of offset ray-parameter. This observation shows that AVA analysis on any of the two kinds of angle gathers is problematic, unless corrective measures are taken (Sava et al., 2001).

The third example concerns a real data set acquired over a region with fairly simple geology (Figure 10). Figure 11 shows image gathers at $x = 7.5$ km. As theoretically predicted, at the imaging step most of the energy is concentrated around zero offset. After the conversion to the angle domain, almost all the events are flat, although some show slight moveout, indicating migration and/or velocity inaccuracies. For this example, too, we can observe the same difference in amplitude behavior of the data-space versus the image-space method as for the synthetic example in Figures 8 and 9.

Figure 12 demonstrates the effect of regularization in the angle domain. In the left panel, we present an angle gather created without regularization ($\epsilon = 0.0$); on the right, we present the same angle gather obtained with regularization ($\epsilon = 1.0$), according to Equation (19). The left panel is populated with artifacts caused by the nonuniform sampling of the ADCIG due to the radial trace transform in the Fourier domain. In contrast, the panel on the right shows fewer artifacts, which makes the reflections much easier to interpret.

The fourth example concerns a 3D common-azimuth (Biondi and Palacharla, 1996) data set from the North Sea (Vaillant et al., 2000). Figure 13 is an inline extracted from the 3D

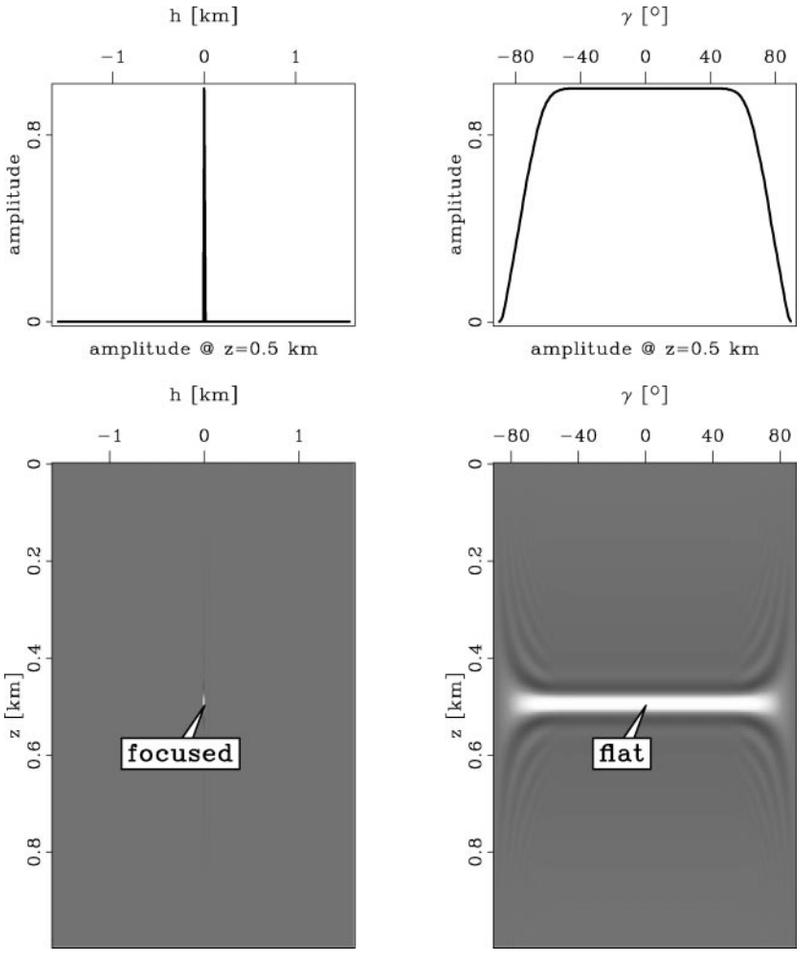

FIG. 6. Ideal offset-domain and angle-domain common-image gathers.

seismic cube and shows a salt body in the middle of the section, surrounded by fairly flat reflectors. Figure 14 shows an image gather at $x = 4.0$ km, presented in the offset domain (left panel) and in the angle domain (right panel). As before, most of the energy is imaged around zero offset, which translates in fairly flat events in the angle gather indicating that both the migration and the velocity model are correct. The geometry of the reflectors in this example are fairly simple, although the waves propagate through a complicated salt area.

DISCUSSION

Several points emphasize the main qualities of our angle-transform method.

1) Our method produces the output as a function of the incidence angle at the reflector, and not as a function of offset ray-parameter. This makes the results more open to interpretation, and potentially allows for consistent quantitative AVA analysis if the amplitudes are handled

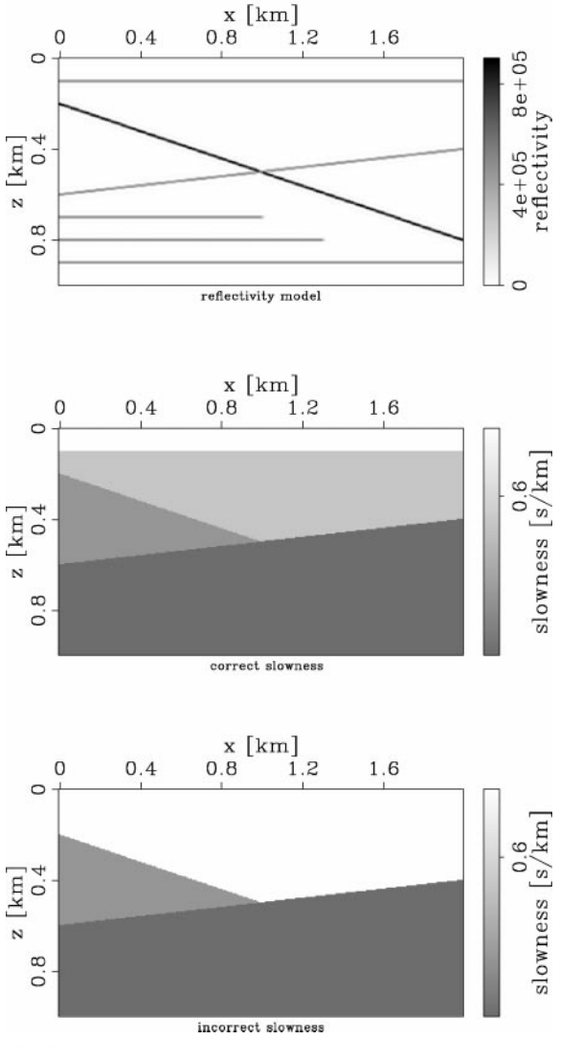

FIG. 7. Two-dimensional synthetic model: from top to bottom, reflectivity model, correct slowness, and incorrect slowness.

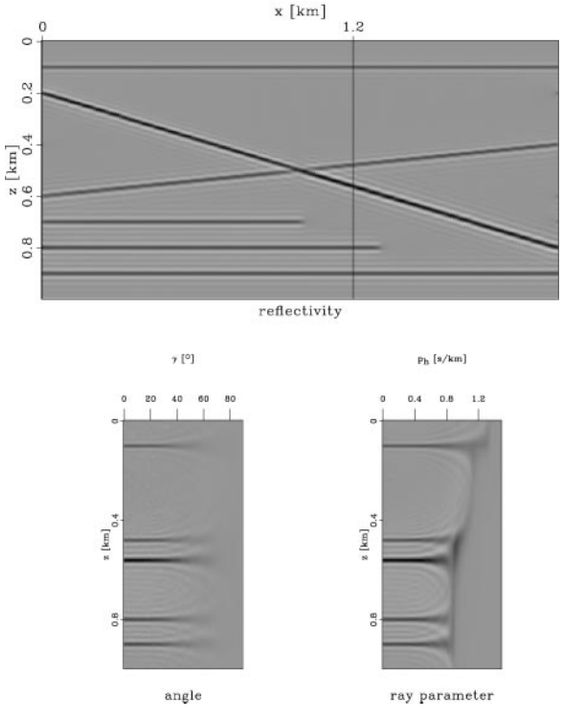

FIG. 8. Synthetic model imaged using the correct velocity model: section obtained by imaging at zero time and zero offset (top), angle gather created in the image space (bottom left), and angle gather created in the data space (bottom right).

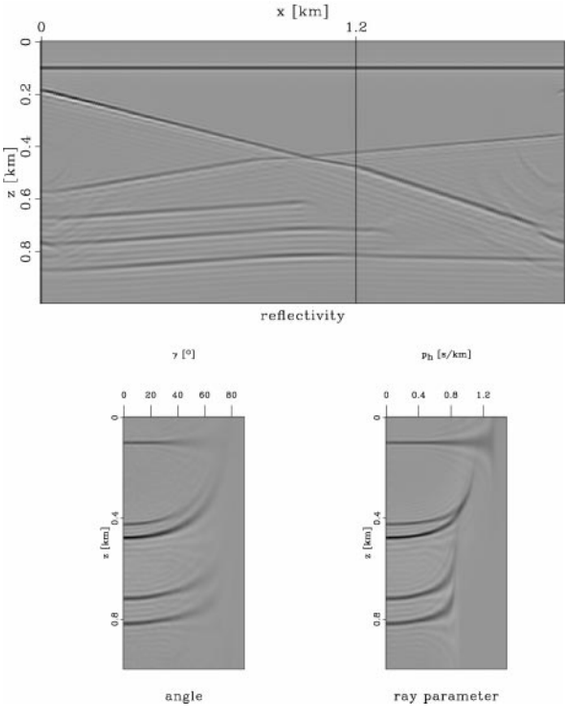

FIG. 9. Synthetic model imaged using the incorrect velocity model: section obtained by imaging at zero time and zero offset (top), angle gather created in the image space (bottom left), and angle gather created in the data space (bottom right).

correctly during migration (Sava et al., 2001). This issue, however, falls outside the scope of this paper.

2) Our method generates angle gathers after and not during migration, thus enabling us to shuttle between the angle and offset domains without remigrating the data. Since the transformation to the angle domain is separated from the migration itself, our method can be used both for shot-geophone downward-continuation migration (as exemplified in this paper, or for shot-profile downward-continuation migration (Rickett and Sava, 2001). The method can also be generalized to the case of converted waves (Rosales and Rickett, 2001) or to two-way propagation methods (Biondi and Shan, 2002).
3) Our method enables inexpensive regularization of the angle domain leading to gathers with events that vary smoothly along the angle axis. The increased S/N ratio helps reveal weak events that would otherwise be harder to interpret.

CONCLUSIONS

We present a new method for computing angle-domain common-image gathers from wave-equation depth-migrated images. We produce angle gathers from migrated images with a process which is completely detached from migration. The output of our image-space method is a function of reflection angle, not of offset ray parameter.

We show that our method is, in essence, a radial trace transform in the Fourier domain and, therefore, equivalent to a slant stack in the space domain. The method is fully applicable to

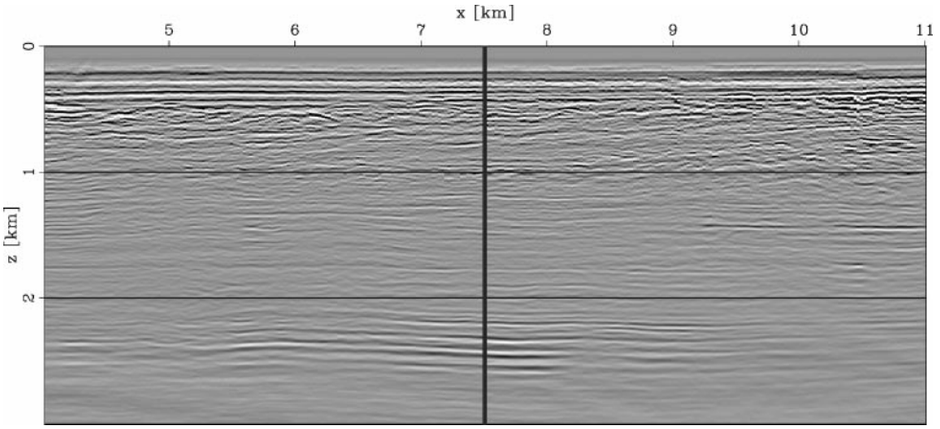

FIG. 10. Two-dimensional real data example: seismic section obtained by imaging at zero time and zero offset.

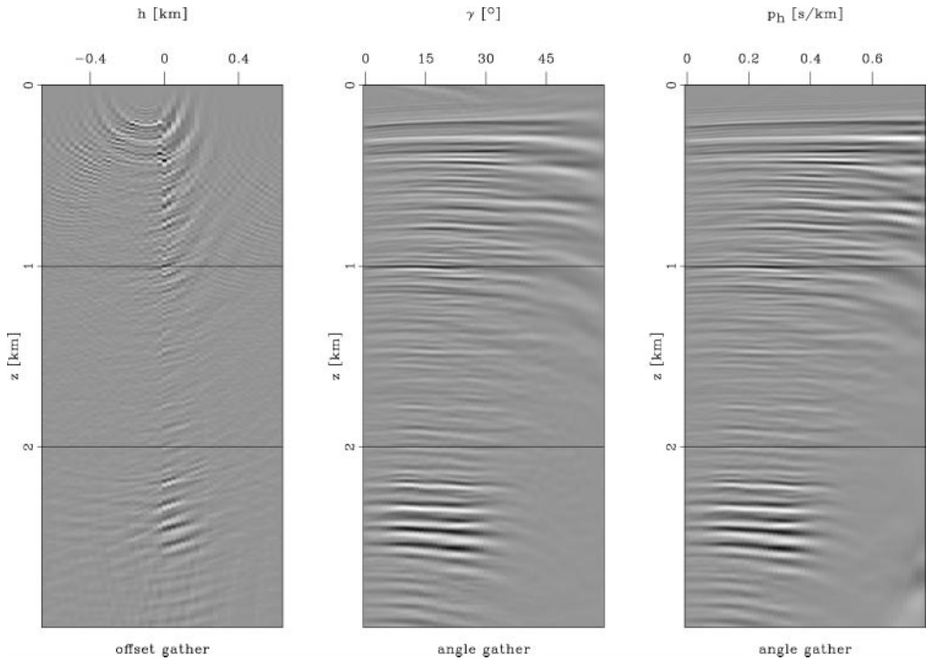

FIG. 11. Two-dimensional real data example: from left to right, offset gather (right panel) and angle gathers, computed in the image space (middle panel) and the data space (right panel).

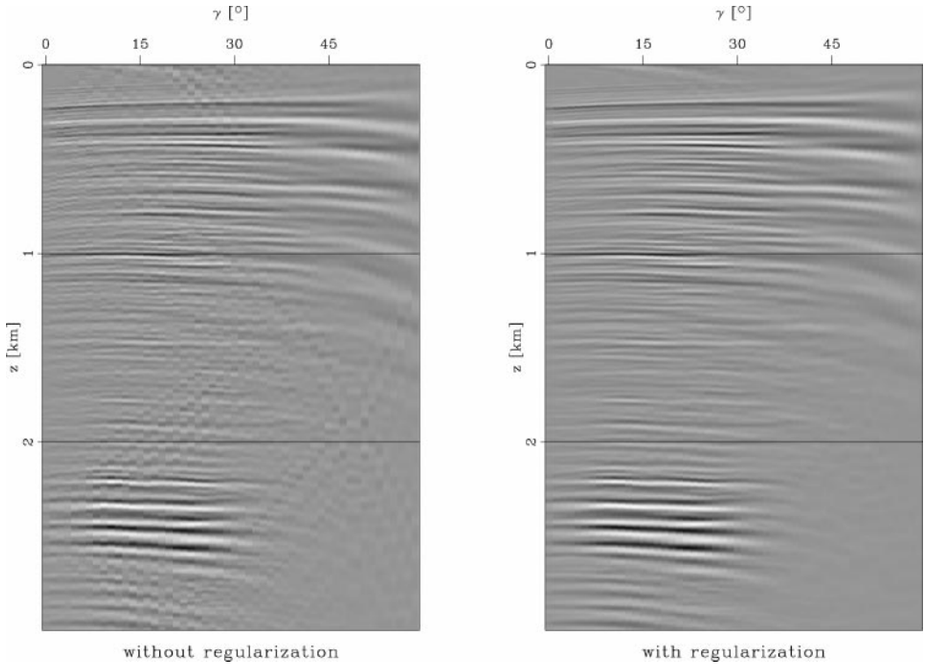

FIG. 12. Two-dimensional real data example: a comparison of an angle gather obtained without regularization (left) and an angle gather obtained with regularization (right).

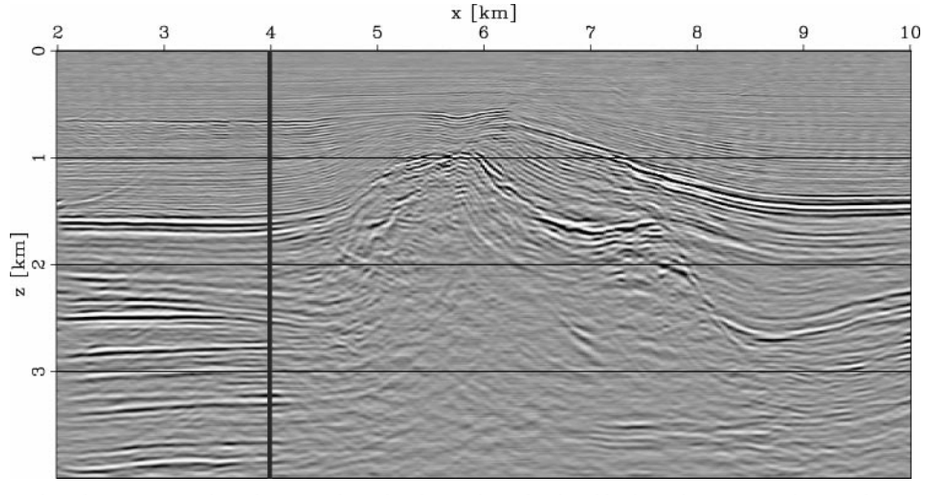

FIG. 13. Three-dimensional common-azimuth example: seismic section obtained by imaging at zero time and zero offset. The vertical line corresponds to the in figure 14.

arbitrary models with high image complexity and lateral velocity variations.

We implement our method using a stretch technique that enables us to include model regularization, thus reducing the artifacts caused by nonuniform sampling due to the Fourier-domain radial-trace transforms. Our method is accurate, fast, robust, easy to implement, and can be used for real 3D prestack data for simple imaging or in applications related to migration velocity analysis and AVA analysis.

ACKNOWLEDGMENTS

We thank TotalFinaElf for the 3D dataset used in our examples. The financial support for this work was provided by the sponsors of the Stanford Exploration Project.

REFERENCES

Biondi, B., and Shan, G., 2002, Prestack imaging of overturned reflections by reverse time migration: 72nd Ann. Internat. Mtg., Soc. Expl. Geophys., Expanded Abstracts, 1284–1287.

Biondi, B., and Palacharla, G., 1996, 3-D prestack migration of common-azimuth data: Geophysics, **61**, 1822–1832.

Brandsberg-Dahl, S., de Hoop, M. V., and Ursin, B., 1999, Sensitivity transform in the common scattering-angle/azimuth domain: 61st Ann. Conf., Eur. Assn. Geosci., Eng., Expanded Abstracts, 1715–1718.

Claerbout, J. F., 1985, Imaging the Earth's interior: Blackwell Scientific Publ.

de Bruin, C., Wapenaar, C., and Berkhout, A., 1990, Angle-dependent reflectivity by means of prestack migration: Geophysics, **55**, 1223–1234.

Fomel, S., 1997, Velocity continuation and the anatomy of residual prestack migration: 67th Ann. Internat. Mtg., Soc. Expl. Geophys., Expanded Abstracts, 1762–1765.

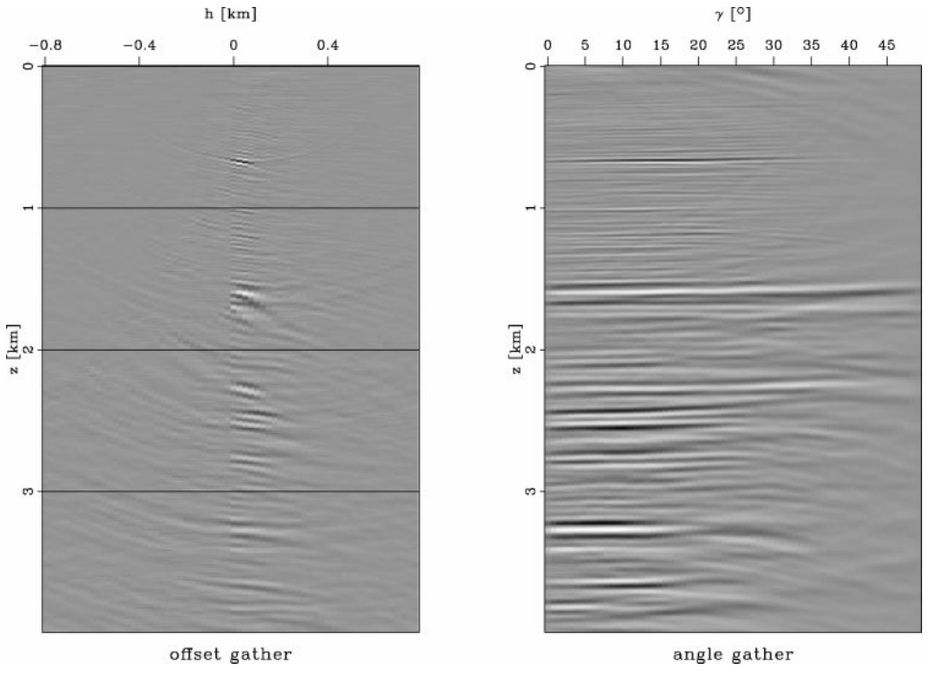

FIG. 14. Three-dimensional common-azimuth example: offset gather (left panel) and angle gather (right panel) corresponding to the vertical line in Figure 13.

Fowler, P., 1997, A comparative overview of prestack time migration methods: 67th Ann. Internat. Mtg., Soc. Expl. Geophys., Expanded Abstracts, 1571–1574.
Golub, G. H., and Van Loan, C. F., 1989, Matrix computations: Johns Hopkins Univ. Press.
Mosher, C., and Foster, D., 2000, Common angle imaging conditions for prestack depth migration: 70th Ann. Internat. Mtg., Soc. Expl. Geophys., Expanded Abstracts, 830–833.
Nolan, C. J., and Symes, W. W., 1996, Imaging and conherency in complex structure: 66th Ann. Internat. Mtg., Soc. Expl. Geophys., Expanded Abstracts, 359–363.
Ottolini, R., 1982, Migration of reflection seismic data in angle-midpoint coordinates: Ph.D. thesis, Stanford Univ.
Prucha, M., Biondi, B., and Symes, W., 1999, Angle-domain common-image gathers by wave-equation migration: 69th Ann. Internat. Mtg., Soc. Expl. Geophys., Expanded Abstracts, 824–827.
Rickett, J., and Sava, P., 2001, Offset and angle domain common-image gathers for shot-profile migration: 71st Ann. Internat. Mtg., Soc. Expl. Geophys., Expanded Abstracts, 1115–1118.
Rosales, D., and Rickett, J., 2001, PS-wave polarity reversal in angle domain common-image gathers: 71st Ann. Internat. Mtg., Soc. Expl. Geophys., Expanded Abstracts, 1843–1846.
Sava, P., Biondi, B., and Fomel, S., 2001, Amplitude-preserved common image gathers by wave-equation migration: 71st Ann. Internat. Mtg., Soc. Expl. Geophys., Expanded Abstracts, 296–299.
Stolk, C., and Symes, W., 2002, Artifacts in Kirchhoff common image gathers: 72nd Ann. Internat. Mtg., Soc. Expl. Geophys., Expanded Abstracts, 1129–1541.
Vaillant, L., Sava, P., Biondi, B., and Calandra, H., 2000, 3-D wave-equation migration of a common-azimuth North Sea dataset: 62nd Mtg., Eur. Assn. Geosci. Eng., Abstracts, 231–235.
Xu, S., Chauris, H., Lambare, G., and Noble, M., 1998, Common angle image gather—A strategy for imaging complex media 68th Ann. Internat. Mtg., Soc. Expl. Geophys., Expanded Abstracts, 1538–1541.
Weglein, A. B., and Stolt, R. H., 1999, Migration-inversion revisted: The Leading Edge, **18**, 950–952.

APPENDIX A

REFLECTION ANGLE FORMULA

In this appendix, we show the derivation of equation (13), which serves as the basis of the frequency-domain angle-gather construction.

In the process of downward continuation, the wavefield appears as a function of four variables: time t, depth z, source lateral position s, and receiver lateral position r. Both the source and receiver assume positions at depth z, where the wavefield is continued (Claerbout, 1985). It is often convenient to replace the variables s and r with the midpoint position $x=(s+r)/2$ and the half-offset $h=(r-s)/2$.

Assuming that the reflection event in the continued wavefield is described by the function $t=t(z,s,r)$, we find from the Snell's law following derivatives:

$$\frac{\partial t}{\partial s}=\frac{\sin(\alpha-\gamma)}{v}, \tag{A-1}$$

$$\frac{\partial t}{\partial r}=\frac{\sin(\alpha+\gamma)}{v}, \tag{A-2}$$

where v is the wave velocity, α is the dip angle, and γ is the reflection angle (Figure 5). The traveltime derivative with respect to the depth of the observation surface z has contributions from the two branches of the reflected ray, as follows:

$$\frac{\partial t}{\partial z}=\frac{\cos(\alpha-\gamma)}{v}+\frac{\cos(\alpha+\gamma)}{v}. \tag{A-3}$$

Equation (A-3) corresponds to the well-known double-square-root equation (Claerbout, 1985). This equation simply reflects the fact that the traveltime increases with increasing depth of the reflector.

Transforming equations (A-1)–(A-3) to the midpoint and half-offset coordinates, we obtain

$$\frac{\partial t}{\partial x} = \frac{\partial t}{\partial s} + \frac{\partial t}{\partial r} = \frac{2\sin\alpha\cos\gamma}{v}, \tag{A-4}$$

$$\frac{\partial t}{\partial h} = \frac{\partial t}{\partial r} - \frac{\partial t}{\partial s} = \frac{2\cos\alpha\sin\gamma}{v}, \tag{A-5}$$

$$\frac{\partial t}{\partial z} = \frac{2\cos\alpha\cos\gamma}{v}. \tag{A-6}$$

At a fixed image location x, we can transform the derivatives of $t(z, x, h)$ to the derivatives of $z(t, x, h)$ by applying the implicit function theorem. Using equations (A-5)–(A-6), we obtain

$$\frac{\partial z}{\partial h} = -\frac{\partial t}{\partial h}\Big/\frac{\partial t}{\partial z} = -\tan\gamma. \tag{A-7}$$

Equation (A-7) corresponds to Equation (13) in the body of the paper. It is important to note that this equation is only suitable for angle-gathers constructed on images obtained by wavefield continuation methods (Figure 5), when h does not represent the surface offset, but half the distance between the downward continued sources and receivers.

In deriving Equation (A-7), we assumed that the velocity v does not change laterally between the source and receiver positions. While this may not be true in general, Equation (A-7) will always be satisfied in the vicinity of zero half offset ($h = 0$). Therefore it is applicable near the focusing points of the downward-continued wavefield.

APPENDIX B

EQUIVALENCE OF RADIAL-TRACE TRANSFORMS TO SLANT STACKS

The Fourier-domain stretch represented by Equation (14) is equivalent to a slant stack in the z-$\mathbf{h}$ domain, where z represents depth and $\mathbf{h}$ represents half offset. Indeed, we can convert an image gather in the offset domain ($\mathbf{H}$) to one in the angle domain ($\mathbf{A}$), using a slant-stack equation of the form

$$\mathbf{A}(z\boldsymbol{\mu}) = \int\!\!\int \mathbf{H}(z + \boldsymbol{\mu}\cdot\mathbf{h}, \mathbf{h})d\mathbf{h}, \tag{B-1}$$

where $\boldsymbol{\mu}$ is a vector describing in three dimensions the direction of the stack.

Fourier transforming equation (B-1) over the depth axis, we obtain

$$\underline{\mathbf{A}}(k_z, \boldsymbol{\mu}) = \int \left[\int\!\!\int \mathbf{H}(z + \boldsymbol{\mu}\cdot\mathbf{h}, \mathbf{h})d\mathbf{h}\right] e^{ik_z z}dz,$$

where the underline stands for a 1D Fourier transform. We can continue by writing the equation

$$\underline{\mathbf{A}}(k_z, \boldsymbol{\mu}) = \int\!\!\int\!\!\int \mathbf{H}(z + \boldsymbol{\mu}\cdot\mathbf{h}, \mathbf{h}) e^{ik_z(z+\boldsymbol{\mu}\cdot\mathbf{h}) - ik_z\boldsymbol{\mu}\cdot\mathbf{h}}d\mathbf{h}dz,$$

where we can rearrange the terms as

$$\underline{\mathbf{A}}(k_z, \boldsymbol{\mu}) = \int\!\!\int \left[\int \mathbf{H}(z + \boldsymbol{\mu}\cdot\mathbf{h}, \mathbf{h}) e^{ik_z(z+\boldsymbol{\mu}\cdot\mathbf{h})}dz\right] e^{-ik_z\boldsymbol{\mu}\cdot\mathbf{h}}d\mathbf{h},$$

which highlights the relation between the 1D Fourier-transformed angle-domain and offset-domain representation of the seismic images:

$$\underline{\mathbf{A}}(k_z, \boldsymbol{\mu}) = \int\!\!\int \underline{\mathbf{H}}(k_z, \mathbf{h}) e^{-ik_z\boldsymbol{\mu}\cdot\mathbf{h}}d\mathbf{h}.$$

We recognize on the right side of the previous equation additional Fourier transforms over the offset axes, and therefore we can write

$$\underline{\mathbf{A}}(k_z, \boldsymbol{\mu}) = \underline{\underline{\underline{\mathbf{H}}}}(k_z, -\boldsymbol{\mu}k_z),$$

where the triple underline stands for the 3D Fourier transform of the offset-domain common-image gather. Finally, defining $-\boldsymbol{\mu}k_z = \mathbf{k}_h$, we can conclude that the 1D Fourier transforms of angle-domain gathers are equivalent to the 3D Fourier transforms of the offset-domain gathers,

$$\underline{\mathbf{A}}(k_z, \boldsymbol{\mu}) = \underline{\underline{\underline{\mathbf{H}}}}(k_z, \mathbf{k}_h), \tag{B-2}$$

subject to the stretch of the offset axis according to the simple law

$$\boldsymbol{\mu} = -\frac{\mathbf{k}_h}{k_z}. \tag{B-3}$$

We can recognize in equation (B-3) the fundamental relation between the reflection angle and the Fourier-domain quantities that are evaluated in wave-equation migration. This equation also shows that the angles evaluated by equation (14) are indeed equivalent to slant stacks on offset-domain ODCIGs. In three dimensions, we could either compute angles for each of the two offset axes with the equations

$$\tan\gamma_x = -\frac{k_{h_x}}{k_z},$$

$$\tan\gamma_y = -\frac{k_{h_y}}{k_z},$$

or we can compute angle gathers as a function of the incidence angle confined to the reflection plane using the relation

$$\tan\gamma = -sign(k_{h_x})\frac{|\mathbf{k}_h|}{k_z}.$$